Depinning assisted by domain wall deformation in cylindrical NiFe nanowires

Chandra Sekhar, M.; Goolaup, S.; Purnama, I.; Lew, W. S.

2014

Chandra Sekhar, M., Goolaup, S., Purnama, I., & Lew, W. S. (2014). Depinning assisted by domain wall deformation in cylindrical NiFe nanowires. Journal of Applied Physics, 115(8), 083913-.

https://hdl.handle.net/10356/104197

https://doi.org/10.1063/1.4867004

Depinning assisted by domain wall deformation in cylindrical NiFe nanowires

M. Chandra Sekhar, S. Goolaup, I. Purnama, and W. S. Lew

Citation: Journal of Applied Physics **115**, 083913 (2014); doi: 10.1063/1.4867004
View online: http://dx.doi.org/10.1063/1.4867004
View Table of Contents: http://scitation.aip.org/content/aip/journal/jap/115/8?ver=pdfcov
Published by the AIP Publishing

Depinning assisted by domain wall deformation in cylindrical NiFe nanowires

M. Chandra Sekhar, S. Goolaup, I. Purnama, and W. S. Lew[a)]
School of Physical and Mathematical Sciences, Nanyang Technological University, 21 Nanyang Link, Singapore 637371

(Received 12 December 2013; accepted 14 February 2014; published online 28 February 2014)

We report on transverse domain wall (DW) depinning mechanisms at the geometrical modulations in NiFe cylindrical nanowires. The DW depinning field and current density always follow opposite trends with diameter modulation. For current driven DW, the depinning current density decreases with increasing notch depth. This interesting behavior arises due to a combination of DW deformation and rotation at the pinning site. With increasing anti-notch height, two distinct depinning mechanisms are observed for both field and current driven DW. Above a critical height, the DW transformation from transverse to vortex configuration leads to a change in the potential barrier. For field-driven, the barrier is lowered, whereas for current-driven, the barrier increases. The increase in the potential barrier for the current driven DW is due to the appearance of an intrinsic pinning within the anti-notch. © *2014 AIP Publishing LLC*. [http://dx.doi.org/10.1063/1.4867004]

INTRODUCTION

The realization of domain wall (DW)-based memory devices[1–3] requires the ability to control the movement of DW in ferromagnetic nanowires. Depending on the size of the nanowire, either transverse or vortex DW is energetically stable.[4,5] It has been shown that in cylindrical nanowires, the dynamics of the transverse DW show unique behaviors that are not found in planar structures.[6–9] For instance, transverse DWs in sub-50 nm cylindrical nanowire is predicted to be free from the Walker breakdown, which is a phenomenon where the internal structure of the DW breaks down due to the application of high field or current.[10,11] Due to geometrical symmetry of the cylindrical nanowires, the lateral motion of the transverse DW in the sub-50 nm nanowire under the influence of an external driving force is accompanied by a rotational motion. This in turn prevents the Walker breakdown.[5,6] Beating the Walker breakdown allows the DW in the cylindrical nanowire to move with much higher speed, as compared to that in planar nanowires. Moreover, the threshold current density that is required to initiate the DW motion is relatively low in cylindrical nanowires. For memory applications, pinning sites have to be created along the nanowires to precisely control the DW motion.[12–17] For cylindrical nanowire, the pinning sites can be realized by introducing a modulation in the diameter of the nanowire in the form of a notch or anti-notch. Although the DW depinning mechanism in the planar structure has been relatively well studied,[12–17] an in-depth understanding of such mechanism at geometrical modulations in the cylindrical nanowire is still elusive.

In this work, we have investigated the field-driven and current-driven depinning mechanisms of transverse DW in cylindrical NiFe nanowires by means of micromagnetic simulation. Using notch as the pinning site, the DW depinning field and the DW depinning current density show opposite behavior with respect to the notch depth. The DW is found to undergo a deformation at the notch structure which helps to lower the depinning current density. For anti-notch pinning site; two types of DW depinning mechanism occur as the dimension is varied. This is in turn is related to the DW transformation process within the anti-notch region.

METHODOLOGY

In this work, a cylindrical NiFe nanowire of 30 nm diameter was chosen to ensure that the transverse DW is energetically stable within the system.[4] The material parameters used in the simulation were $Ni_{80}Fe_{20}$: Saturation magnetization (M_s) = 800×10^3 A/m, exchange stiffness constant (A_{ex}) = 1.3×10^{-11} J/m, and magnetocrystalline anisotropy $k = 0$. We used the object oriented micromagnetic framework code (OOMMF)[18] extended by incorporating the spin transfer torque term to the Landau–Lifshitz–Gilbert (LLG) equation.[19] The Gilbert damping constant (α) and the non adiabatic constant (β) were fixed at 0.005 and 0.04, respectively. The notch and anti-notch are cylindrically symmetric and concentric regions with respect to the nanowire, as schematically shown in Figure 1(a). The length of the modulated regions (i.e., notch, anti-notch) was kept constant at 100 nm while the diameter was varied. The depth of the notch (N_d) or the height of the anti-notch (AN_h) is defined as the difference in the diameter between the nanowire and the notch/anti-notch. The length of the nanowire is 2 μm, and the notch/anti-notch was positioned at the center of the nanowire and designated as the center of coordinate ($x = 0$). A DW was initially relaxed at $x = -700$ nm with respect to the center of the nanowire.

RESULTS AND DISCUSSION

To investigate the energy landscape that is present at the notch and anti-notch in the cylindrical nanowire, we have analyzed the DW energy as a function of position while it is

[a)]Author to whom correspondence should be addressed. Electronic mail: wensiang@ntu.edu.sg

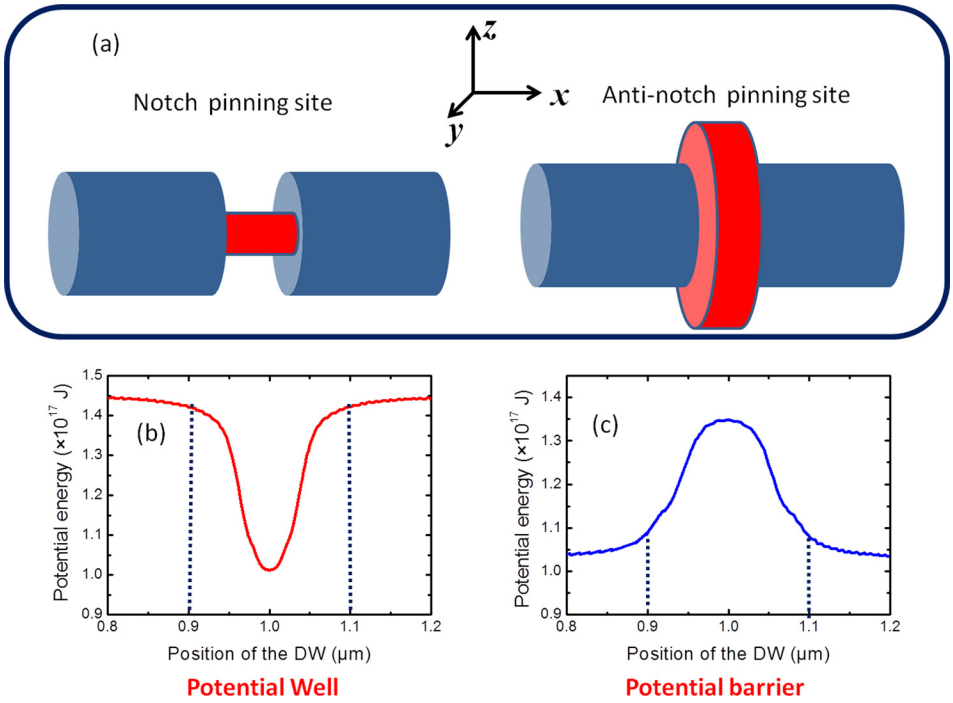

FIG. 1. (a) Schematic diagram of the cylindrical nanowire simulation model with symmetrical geometrical modulations, i.e., notch (left) and anti-notch (right) pinning sites. DW potential energy as a function of the position along the nanowire for (b) notch and (c) anti-notch.

driven by a magnetic field of 1 kOe. The depth of the notch N_d, (or the height of the anti-notch AN_h) is fixed at 5 nm. With applied magnetic field, the potential energy landscape can be obtained by subtracting the Zeeman energy from the total energy of the system.[20] For the notch structure, the potential energy drops when the DW is within the notch structure, as seen in Figure 1(b), whereas for the anti-notch, the potential energy increases when the DW is within the anti-notch as seen in Figure 1(c). This implies that the two pinning sites have different energy properties—the notch acts as a potential well while the anti-notch acts as a potential barrier. The pinning strength for the notch is relatively higher as compared to that of the anti-notch, as revealed by the magnitude of the potential well (0.43×10^{-17} J), as compared to the potential barrier (0.32×10^{-17} J), for the same magnitude of the N_d and AN_h.

FIELD-INDUCED TRANSVERSE DW DEPINNING

Figure 2(a) shows the dynamic behavior of the field-driven DW in a nanowire with a notch depth (N_d) of 20 nm. The magnetic field was increased in steps of 5 Oe to estimate the depinning field. The magnetization component along the nanowire long axis (x-axis), m_x indicates the translational motion of the DW; while the magnetization component along the z-axis, m_z can be interpreted to indicate the DW rotation around the longitudinal axis. The DW dynamics plot is analyzed into three regions: Region I is the DW dynamics before the DW enters the notch, region II is when the DW is within the notch, and region III is after the DW has left the notch. In region I, the oscillating m_z component and the linearly increasing m_x component indicate that the DW rotates and moves linearly along the nanowire before it reaches the modulated region. The DW is not immediately pinned when it enters the notch region, instead, its size reduces to accommodate the smaller diameter of the notch structure. The DW is pinned at the right edge of the notch as shown in the magnetization configuration in Figure 2(b). The DW pinning can be seen from the constant m_x with respect to simulation time in region II. The DW rotational motion also changes from sustained rotations to discontinuous rotations as shown by the m_z plot. The DW pinning in the notch structure can be understood from the dependence of DW energy on the DW size. From the DW theory, DW energy (E_{DW}) is defined as[21]

$$E_{DW} = \frac{\pi^2 A}{\delta} + K\delta,$$

where A is the exchange stiffness constant, K is the anisotropy energy density, and δ is the DW width (lateral size). Due to the dominance of the second term, the DW energy is almost proportional to the DW width. The DW energy is lower within the notch due to the reduced size. The DW is pinned at the notch as it is unable to restore the energy and structure to move forward from the notch. As the DW gradually gains sufficient energy from the Zeeman energy, it depins and enters the nanowire as shown in Figure 2(c). The field required for depinning is found to be 1.8 KOe. In region III, the m_z component starts to oscillate again indicating that the DW has regained its rotational motion after it has depinned from the notch.

To study the effect of notch depth on the depinning field, the notch depth (N_d) was varied from 20 nm to 5 nm (corresponding to the diameter 10 nm to 25 nm). As shown in Figure 2(d), the depinning field increases as the notch depth is increased. This implies that the depth of the potential well increases with deeper notch. The DW size within the notch is directly related to the notch diameter. When the diameter of the modulated region is reduced, the size of the DW is also scaled down, and the DW energy decreases correspondingly. Hence, the field that is required to restore the DW energy via Zeeman contribution increases. Such results are

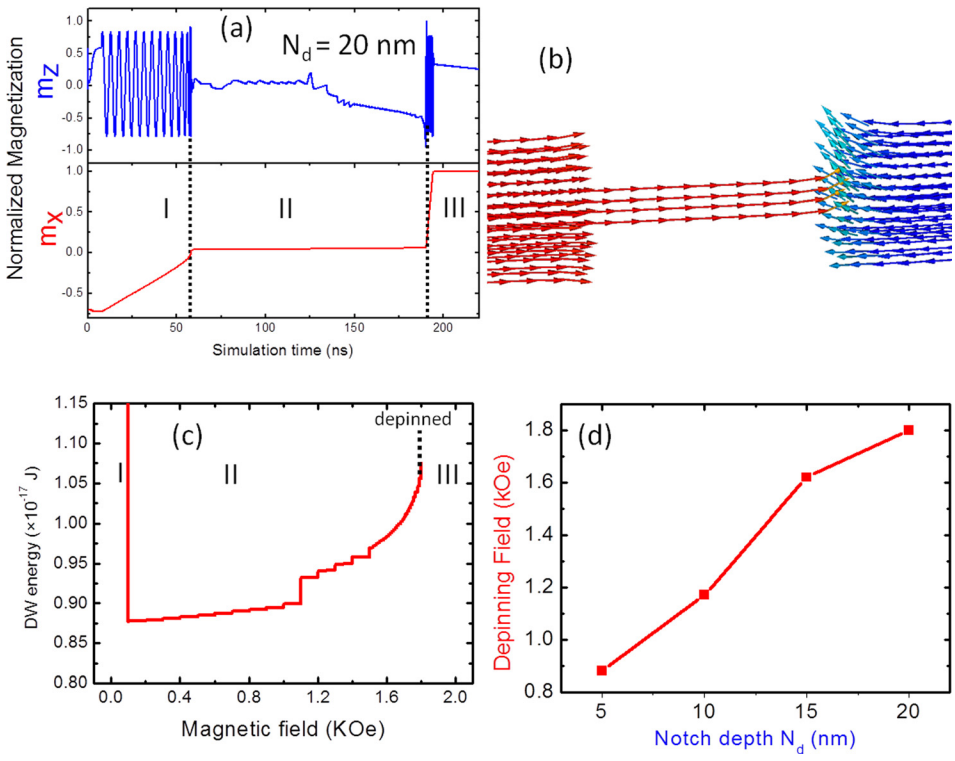

FIG. 2. (a) Field-driven DW motion in cylindrical nanowire with a notch ($N_d = 20$ nm). The magnetization along the long axis (m_x) and around the long axis (m_z) corresponds to the DW translational and rotational motion in the cylindrical nanowire, respectively. (b) The magnetization configuration of the nanowire while the DW is pinned at the notch. (c) The variation in the DW potential energy as a function of the external magnetic field. (d) DW depinning field as a function of the notch depth.

in agreement with the conventional field-induced transverse DW depinning process in planar nanowire structures,[13,14] where a notch with deeper profile produces a stronger pinning potential.

In the case of anti-notch, the DW follows two distinct depinning mechanisms as shown in Figure 3(a) (region P and Q), in accordance to the anti-notch height. When the anti-notch height $(AN_h) \leq 15$ nm, the depinning field increases linearly with the anti-notch height. For anti-notch height $AN_h > 15$ nm, a reverse trend is seen where the depinning field starts to drop. To analyze the two depinning mechanisms, the field-dependent demagnetization energy values and the magnetization configurations were extracted, as shown in Figures 3(b) and 3(c). When $AN_h \leq 15$ nm, the transverse DW maintains its transverse configuration when it is trapped inside the anti-notch, as shown in the inset of Figure 3(b). When the applied field is increased, the transverse DW starts to acquire additional energy from the Zeeman contribution to break free from the anti-notch. However, when the height of the anti-notch is greater than 15 nm, a different behavior is observed as the transverse DW transforms into a vortex configuration. For $AN_h > 20$ nm, the overall diameter of the pinning segment becomes larger than 50 nm, which changes the stable configuration of the DW from transverse to vortex state. The rapid drop of the demagnetization energy as shown in Figure 3(c) confirms the DW transformation. The drop of the demagnetization energy lowers the potential barrier height. In addition, mobility of the vortex DWs is higher compared to the transverse DW when driven by magnetic field.[4] The higher mobility of the vortex DW, along with the drop in the barrier height, allows the DW to depin at a lower field. The vortex DW transforms back into the transverse configuration after leaving the anti-notch structure.

CURRENT-INDUCED TRANSVERSE DW DEPINNING

When under the influence of spin polarized current, the transverse DW moves due to the localized momentum transfer from the spin transfer torque (STT). The modulated regions of the nanowire causes a change in the current density distribution as it flows within the nanowire. In our simulations, though we do consider the variation of the current density at the modulated region, the critical current density for the DW depinning is taken as the current density that is applied to the nanowire (non-modulated regions). The dynamic behavior of a current-driven DW in a nanowire with a notch, $N_d = 20$ nm is shown in Figure 4(a). Similar to the field-driven DW analysis, the plot is analyzed in three distinct regions. In region I, where the DW moves towards the notch structure, the DW translational motion (m_x) is not linear but follows an oscillatory behavior. The oscillation is analogous to a damped harmonic motion of a particle that is under the influence of two oppositely-directed forces. In this case, the DW is influenced by the spin-transfer torque from the current and the magnetic stray fields. The origin of the stray fields is the spins that exist at the boundary of the modulation region, as shown by the simulated spin configuration in Figure 4(b). The m_z plot also shows an oscillatory behavior which indicates that the DW rotates around the longitudinal axis. In region II, where the DW is within the notch structure, the constant m_x value indicates there is no DW translational motion along the long axis as the DW is trapped at the right edge of the notch. However, unlike the

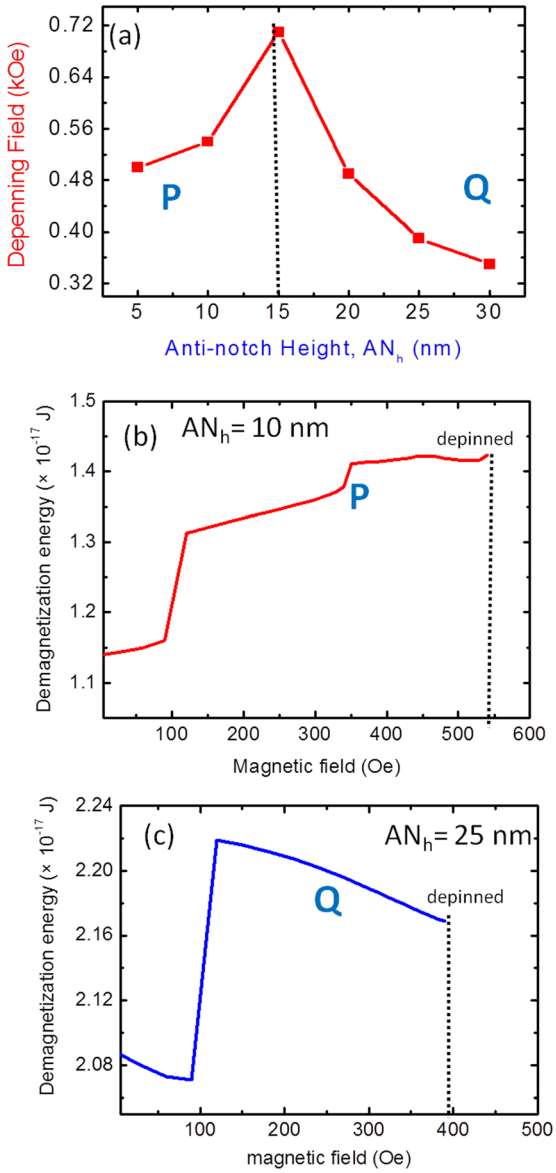

FIG. 3. (a) Domain wall depinning field as a function of the height of anti-notch. (b) Demagnetization energy of the field-induced DW motion in the anti-notch ($AN_h = 10$ nm) corresponding to region P. Inset shows the magnetization configuration of the DW within the anti-notch. (c) Demagnetization energy of the field-induced DW motion in the anti-notch ($AN_h = 25$ nm) corresponding to region Q. Inset shows the magnetization configuration of the DW within the anti-notch.

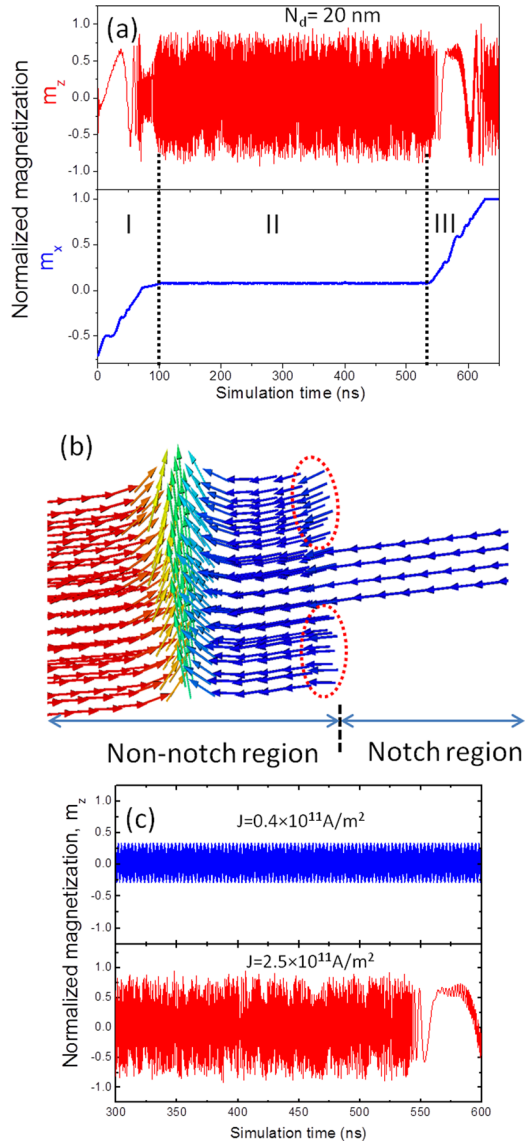

FIG. 4. (a) Current-driven DW motion in cylindrical nanowire with a notch ($N_d = 20$ nm). The magnetization of nanowire along the long axis (m_x) and around the long axis (m_z) represent the DW translational and rotational motion in the nanowire, respectively. (b) The magnetization configuration of the nanowire with a DW pinned at the notch. Dotted red circles indicate spins present at the boundary of the notch structure, which generate stray fields and affect the DW motion. (c) The DW rotation (m_z) at the pinning site as a function of the simulation time for two different current densities. At lower current density (0.4×10^{11} A/m^2), the m_z oscillation is near symmetric, and the amplitude is lower, indicating a stable DW rotation at the pinning site. At higher current density (2.5×10^{11} A/m^2), the m_z oscillation is asymmetric, and the amplitude is larger, indicating the DW depinning process.

field-driven case, the m_z component continues to oscillate, even though the DW is pinned at the notch. The STT effect provides the energy required to sustain the DW rotation, so as to reach an equilibrium condition.[22] In the field-driven case, the DW rotational motion is not sustained as the torque exerted by the magnetic field decreases in time due to the damping term. However, in the current driven case, the STT effect compensates the damping term, and the system achieves an equilibrium condition where the magnetization dynamics can be sustained.[23–26]

Two types of DW rotational motions take place at the pinning site depending on the applied current density, as shown in Figure 4(c). At a current density $J = 0.4 \times 10^{11}$ A/m^2, the rotational m_z component has a near symmetric amplitude, which indicates that the system is at a relatively stable state (lower energy), thus the DW cannot depin from the notch. At a current density $J = 2.5 \times 10^{11}$ A/m^2, the m_z component has a higher but rather asymmetric amplitude. The asymmetric DW rotational motion maintains a higher energy state and that enables the DW to depin from the notch. For 20 nm-deep notch, the critical current density is 2.5×10^{11} A/m^2, which is one order smaller as compared to the typical depinning current density in the planar nanowires. In region III, after the DW leaves the notch structure, the DW continues the oscillatory behavior.

Different notch dimensions were investigated to understand the effect of notch depth on the depinning current

density. Simulation results show that when the notch depth, N_d is varied from 5 nm to 20 nm, the depinning current density decreases, as shown in Figure 5(a). Such behavior is opposite to that of the field-driven case, where the depinning field increases with the notch depth. The magnetization configurations of the transverse DW when it is pinned at the notch of different depth are shown in Figure 5(b). For the 5-nm-deep notch, the transverse DW is shown to retain its transverse configuration, albeit with a smaller DW width. For the 20-nm-deep notch, the DW width is larger because of shape deformation. The transverse DW shape variation corresponds to energy difference between two systems, which affects the depinning process consequently. Figure 5(c) shows the total energy of the system as a function of simulation time for the two notches (5 nm and 20 nm deep), with an applied current density of $J = 2.5 \times 10^{11}$ A/m^2. The plot shows that the DW total energy drops significantly when the transverse DW enters the notch. If the applied current density is less than the critical value, the transverse DW is pinned next to the notch with its profile and energy partially restored. For the 5-nm-deep notch, the DW is able to restore its transverse shape, however it only yields approximately 50% of its initial energy because of the smaller DW width. Hence, it is unable to depin from the notch even with the assistance of the STT effect. For the 20-nm-deep notch, the DW is able to restore approximately 70% of the initial energy because it gains additional energy from the shape deformation. The contribution from the STT effect increases the shape deformation of the transverse DW. The high energy state of the system coupled with the DW deformation eventually leads to a complete depinning process. As the applied current density is increased further, the DW shape deformation occurs faster, resulting in a shorter depinning time. The unique behavior of lower depinning current density at deeper notch is observed only in cylindrical nanowires. In planar nanowires, the depinning current density is always reported to increase with a deeper notch.[27,28] The DW in the planar nanowire is hindered from rotation due to the shape anisotropy which forces it to be depinned at a higher current density. In cylindrical nanowires, the DW rotation which allows it to depin at a lower current density.

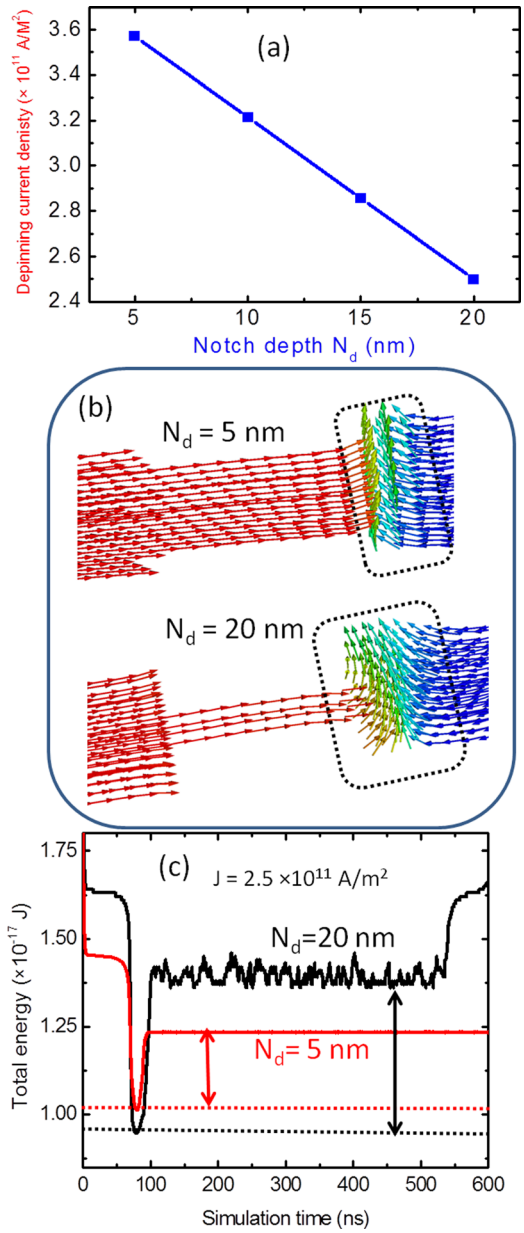

FIG. 5. (a) DW depinning current density as a function of notch depth. (b) Snapshot images of the magnetization configuration of the DW pinned at the notch of two different depths 5 nm and 20 nm. (c) Total energy of the system as a function of time for two different notch depths when the DW is driven through the notch by same current density ($J = 2.5 \times 10^{11}$ A/m^2).

Figure 6(a) shows the translational motion of the current-driven DW along the nanowire axis (m_x component) as it propagates across an anti-notch of $AN_h = 5$ nm. The DW reaches an equilibrium position at the left edge of the anti-notch as shown in the inset of Figure 6(a). The depinning current density is plotted as a function of the anti-notch height in Figure 6(b). The plot shows that two DW depinning mechanisms are involved as the anti-notch height is increased. In region A ($AN_h \leq 15$ nm), the depinning current density drops when the anti-notch height is increased from 5 nm to 15 nm. The simulated magnetization configuration (inset of Figure 6(a)) reveals that the pinned DW retains its transverse configuration but is deformed at the boundary of the anti-notch. The degree of the DW deformation at the 15-nm-high anti-notch is higher than that at the 5-nm-high anti-notch, which leads to a lower depinning current density. In region B ($AN_h > 15$ nm), however, the depinning current density increases with increasing anti-notch height, therefore a different depinning mechanism is expected. When the anti-notch height is increased beyond 15 nm (which results in a modulated region with a total diameter more than 45 nm), the spins within the anti-notch start to follow the cylindrical shape to reduce the demagnetization energy. The current-driven transverse DW is then transformed into a vortex DW inside the anti-notch to follow the spins orientations. Shown in Figure 6(c) are the cross-sectional magnetization configurations of the DW within an anti-notch with a height of $AN_h = 30$ nm at four different stages. Initially, at $t = 0$ ns, the spins of the anti-notch at remanence are found to be rotating in a clock-wise direction. When the transverse DW enters the anti-notch ($t = 86$ ns), the DW is then transformed into a

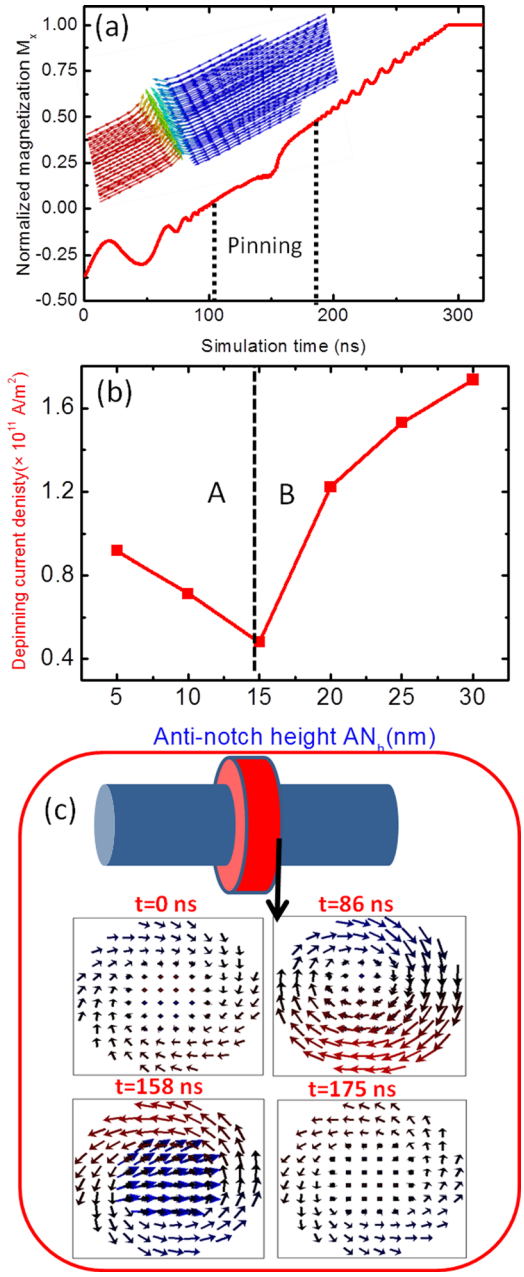

FIG. 6. (a) Current-driven DW motion in the cylindrical nanowire with an anti-notch. Inset shows the DW pinned at anti-notch. (b) Depinning current density as a function of the anti-notch height. (c) The evolution of the vortex magnetization at the boundary of the anti-notch ($AN_h = 30$ nm) at four different stages during the DW depinning through the anti-notch. The chirality of the vortex configuration switches from clock-wise to counter clock-wise during the DW depinning.

vortex DW with clock-wise chirality. However, due to the spin-polarized current,[5] the DW changes its chirality from clock-wise to counter clock-wise orientation at $t = 158$ ns. Finally, the DW is depinned at $t = 175$ ns. The forward torque ($+x$ direction) from the spin-polarized current is enhanced when the vortex DW has a counter clock-wise chirality,[5] which allows it to be depinned from the anti-notch. As the anti-notch height is increased beyond 15 nm, the vortex configuration of the DW inside the anti-notch becomes more pronounced, and, thus, it requires higher current density to switch its chirality from clockwise to anti-clockwise in order to be depinned from the anti-notch.

CONCLUSION

When a DW propagates in a nanowire with modulated regions, it perceives a notch structure as a potential well and an anti-notch structure acts a potential barrier. In their motions, the transverse DWs are pinned at these modulated structures. The pinning potential is found to increase with notch depth when the motion is field-driven, but an opposite behavior is observed when it is driven by current. Such observation is attributed to the DW deformation and rotational behavior within the notch, which contributes to the depinning process. The degree of the DW deformation is larger at a deeper notch, and it assists to lower the depinning current density. In the case of anti-notch, the DW transforms from transverse to vortex configuration as the anti-notch diameter increases. Such DW transformations induce a change in the height of the DW pinning potential. Anti-notch acts as a weak pinning site compared to the notch irrespective of the driving mechanism.

ACKNOWLEDGMENTS

This work was supported by the Singapore National Research Foundation CRP Grant (Non-volatile memory and logic integrated circuit devices, NRF2011NRF-CRP002-014).

[1]X. Jiang, L. Thomas, R. Moriya, M. Hayashi, B. Bergman, C. Rettner, and S. S. P. Parkin, Nat. Commun. **1**, 25 (2010).
[2]R. Moriya, S. S. P. Parkin, and L. Thomas, U.S. Patent, 0,046,268A (25 February 2010).
[3]S. S. P. Parkin, M. Hayashi, and L. Thomas, Science **320**, 190 (2008).
[4]R. Wieser, U. Nowak, and K. D. Usadel, Phys. Rev. B **69**, 064401 (2004).
[5]R. Wieser, E. Y. Vedmedenko, P. Weinberger, and R. Weisendanger, Phys. Rev. B **82**, 144430 (2010).
[6]M. Yan, A. Kakay, S. Gliga, and R. Hertel, Phys. Rev. Lett. **104**, 057201 (2010).
[7]M. Franchin, A. Knittel, M. Albert, D. S. Chernyshenko, T. Fischbacher, A. Prabhakar, and H. Fangohr, Phys. Rev. B **84**, 094409 (2011).
[8]H. Forster, T. Schrefl, W. Scholz, D. Suess, V. Tsiantos, and J. Fidler, J. Magn. Magn. Mater. **249**, 181 (2002).
[9]R. Hertel, J. Magn. Magn. Mater. **249**, 251 (2002).
[10]M. Hayashi, L. Thomas, C. Rettner, R. Moriya, and S. S. P. Parkin, Nat. Phys. **3**, 21 (2007).
[11]G. S. D. Beach, C. Nistor, C. Knutson, M. Tsoi, and J. L. Erskine, Nature Mater. **4**, 741–744 (2005).
[12]D. Atkinson, D. S. Eastwood, and L. K. Bogart, Appl. Phys. Lett. **92**, 022510 (2008).
[13]M. Klaui *et al.*, Appl. Phys. Lett. **87**, 102509 (2005).
[14]S. Goolaup, S. C. Low, M. C. Sekhar, and W. S. Lew, J. Phys.: Conf. Ser. **266**, 012079 (2011).
[15]D. Petit, A.-V. Jausovec, H. T. Zeng, E. Lewis, L. O' Brien, D. Read, and R. P. Cowburn, Phys. Rev. B **79**, 214405 (2009).
[16]M. C. Sekhar, S. Goolaup, I. Purnama, and W. S. Lew, J. Phys. D: Appl. Phys. **44**, 235002 (2011).
[17]S.-H. Huang and C.-H. Lai, Appl. Phys. Lett. **95**, 032505 (2009).
[18]M. Donahue and D. G. Porter, *OOMMF User's Guide, Version 1.0, Interagency Report NISTIR 6376* (National Institute of Standard and Technology, Gaithersburg, MD, 1999).
[19]OOMMF Extension for Current-induced Domain Wall Motion developed by IBM Research, Zurich, see http://www.zurich.ibm.com/st/magnetism/spintevolve.html for the code implementing the two spin transfer torque terms (adiabatic and non-adiabatic) modifying the LLG equation.
[20]M. Hayashi, L. Thomas, C. Rettner, R. Moriya, X. Jiang, and S. S. P. Parkin, Phys. Rev. Lett. **97**, 207205 (2006).
[21]C. H. Marrows, Adv. Phys. **54**(8), 585 (2005).
[22]M. Franchin, T. Fischbacher, G. Bordignon, P. de Groot, and H. Fangohr, Phys. Rev. B **78**, 054447 (2008).

[23]S. I. Kiselev, J. C. Sankey, I. N. Krivorotov, N. C. Emley, R. J. Schoelkopf, R. A. Buhrman, and D. C. Ralph, Nature **425**, 380 (2003).
[24]E. Martinez, L. Torres, and L. Lopez-Diaz, Phys. Rev. B **83**, 174444 (2011).
[25]T. Ono and Y. Nakatani, Appl. Phys. Exp. **1**, 061301 (2008).
[26]K. Matsushita, J. Sato, and H. Imamura, J. Appl. Phys. **105**, 07D525 (2009).
[27]T. Komine, H. Murakami, T. Nagayama, and R. Sugita, IEEE Trans. Magn. **44**, 2516 (2008)
[28]A. Himeno, S. Kasai, and T. Ono, Appl. Phys. Lett. **87**, 243108 (2005)